Double-Exchange and Vibronic Coupling in Mixed-Valence Systems. Electronic Structure of $[Fe_4S_4]^{3+}$ Clusters in High-Potential Iron Protein and Related Models

Emile L. Bominaar, Sergueï A. Borshch,*,† and Jean-Jacques Girerd*

Contribution from the Laboratoire de Chimie Inorganique, URA CNRS 420, Institut de Chimie Moléculaire d'Orsay, Université Paris-Sud, 91405 Orsay, France

Received August 2, 1993. Revised Manuscript Received January 6, 1994®

Abstract: The origin of the pair-delocalized ground state of spin $S = 1/2$, observed in the chemically symmetric, mixed-valence $[Fe_4S_4]^{3+}$ cores in the high-potential iron protein (HiPIP) and its synthetic analogues, is analyzed in the framework of an effective Hamiltonian model, comprising terms for excess-electron transfer (leading to double-exchange coupling of the paramagnetic Fe(III) cores), vibronic coupling (trapping the excess electron), and Heisenberg–Dirac–Van Vleck exchange. The adiabatic potential surfaces of the system d^5-d^5-d^5-d^6 are determined, and their extremal points, corresponding to definite electron distributions, are ascertained. The electron distributions depend essentially on the ratio of the transfer parameter and vibronic trapping energy, $\beta/(\lambda^2/2\kappa)$. For small ratios, the excess electron is site-trapped; for ratios of larger magnitude (≥ 1), the delocalization behavior depends on the nature of the electronic state considered. The transfer Hamiltonian has for $\beta < 0$ an orbitally nondegenerate ground state of high spin ($S = 19/2$), in which the excess electron is uniformly distributed over the four sites. However, for $\beta > 0$, the transfer interaction stabilizes a highly orbital- and spin-degenerate electronic ground state, including spin levels ranging from $S = 1/2$ to $17/2$. The degeneracy is removed by vibronic interaction, leading to broken-symmetry, pair-delocalized states which appear in the energy order $E(1/2) < E(3/2) < \ldots$. Inhomogeneous HDVV exchange, arising from differences in the coupling parameters for ferrous–ferric (J) and ferric–ferric (J_1) interactions, has little effect on the composition of the broken-symmetry states but has a great impact on state energy. The spin structures of the two lowest broken-symmetry states of the total Hamiltonian are similar to those inferred from spectroscopic studies of HiPIP and synthetic analogues thereof.

Introduction

The high-potential iron protein (HiPIP) from *Chromatium vinosum* belongs to a class of iron–sulfur proteins which contain one $[Fe_4S_4]$ core per molecule. X-ray studies of the protein show that the active center consists of four iron ions, each in a distorted tetrahedral environment of three bridging sulfur atoms and a fourth sulfur ligand from a terminal cysteine residue (Figure 1).[1] Cores of this type are also found in four-iron and eight-iron ferredoxins. The iron–sulfur proteins occur in three different redox states: $[Fe_4S_4]^+/[Fe_4S_4]^{2+}/[Fe_4S_4]^{3+}$, where the first two oxidation levels are present in ferredoxins, while the latter two are found in HiPIP.[2] The three oxidation levels correspond to mixed-valence states with the formal valencies 3Fe(II) + 1Fe(III)/2Fe(II) + 2Fe(III)/1Fe(II) + 3Fe(III), respectively, the iron ions being in states of high spin. The electronic states can be represented as structures composed of four high-spin Fe(III) cores, accommodating one or several "excess" electrons.

The oxidized HiPIP has been studied, just as the other systems, by a wide range of spectroscopic techniques, including Mössbauer, EPR, ENDOR, NMR, and MCD.[3-14] These studies provide data relevant to the understanding of both the magnetic properties and the distribution of the electronic charge in the iron–sulfur clusters. The EPR investigations furnish signals characteristic

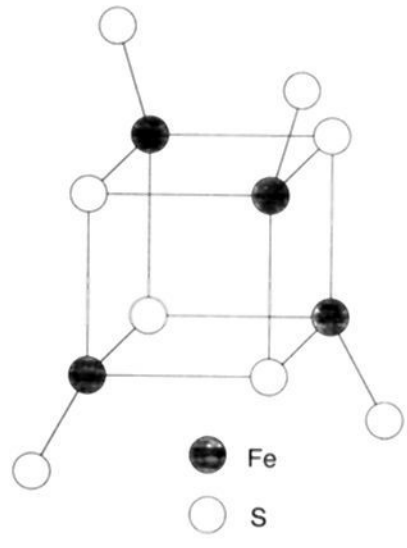

Figure 1. Schematic representation of the tetranuclear "cubane" $[Fe_4S_4]$ cluster in high-potential iron protein.

† Institut de Recherches sur la Catalyse, CNRS, 69626 Villeurbanne cedex, France.

® Abstract published in *Advance ACS Abstracts,* March 15, 1994.

(1) Carter, C. W.; Kraut, J.; Freer, S. T.; Alden, R. A.; Sieker, L. C.; Adman, E. T.; Jensen, L. H. *Proc. Natl. Acad. Sci. U.S.A.* **1972**, *69*, 3526–3529.

(2) Carter, C. W. In *Iron-Sulfur Proteins*; Lovenberg, W., Ed.; Academic Press: New York, 1977; Vol. 3, pp 157–204.

(3) Antanaitis, B. C.; Moss, T. H. *Biochim. Biophys. Acta* **1975**, *405*, 262–279.

(4) Peisach, J.; Orme-Johnson, N. R.; Mims, W. B.; Orme-Johnson, W. H. *J. Biol. Chem.* **1977**, *252*, 5643–5650.

(5) Evans, M. C. W.; Hall, D. O.; Johnson, C. E. *Biochem. J.* **1970**, *119*, 289–291.

(6) Dickson, D. P. E.; Johnson, C. E.; Cammack, R.; Evans, M. C. W.; Hall, D. O.; Rao, K. K. *Biochem. J.* **1974**, *139*, 105–108.

(7) Middleton, P.; Dickson, D. P. E.; Johnson, C. E.; Rush, J. D. *Eur. J. Biochem.* **1980**, *104*, 289–296.

(8) Anderson, R. E.; Anger, G.; Petersson, L.; Ehrenberg, A.; Cammack, R.; Hall, D. O.; Mullinger, R.; Rao, K. K. *Biochim. Biophys. Acta* **1975**, *376*, 63–71.

(9) Phillips, W. D.; Poe, M.; McDonald, C. C.; Bartsch, R. G. *Proc. Natl. Acad. Sci. U.S.A.* **1970**, *67*, 682–687.

(10) Nettesheim, D. G.; Meyer, T. E.; Feinberg, B. A.; Otvos, J. D. *J. Biol. Chem.* **1983**, *258*, 8235–8239.

(11) Johnson, M. K.; Thomson, A. J.; Robinson, A. E.; Rao, K. K.; Hall, D. O. *Biochim. Biophys. Acta* **1981**, *667*, 433–451.

(12) Spiro, T. G.; Hare, J. W.; Yachandra, V. K.; Gewirth, A.; Johnson, M. K.; Remsen, E. In *Metal Ions in Biology*; Spiro, T. G., Ed.; Wiley-Interscience: New York, 1982; Vol. 4, pp 407–423.

(13) Papaefthymiou, V.; Girerd, J.-J.; Moura, I.; Moura, J. J. G.; Münck, E. *J. Am. Chem. Soc.* **1987**, *109*, 4703–4710.

(14) Trautwein, A. X.; Bill, E.; Bominaar, E. L.; Winkler, H. *Structure and Bonding*; Springer Verlag: Berlin, Heidelberg, 1991; Vol. 78, pp 1–95 and references therein.

0002-7863/94/1516-5362$04.50/0

for total spin $S = 1/2$, having anisotropic g values with an average $g_{av} = 2.05$.[3,4] Mössbauer spectroscopic studies reveal that the four iron sites occur in two internally equivalent pairs.[5-7] The pair of iron centers designated by α contains the major part of the excess-electron charge, which is equally distributed over the two sites therein, leading to the formal oxidation states $Fe^{(2.5+\epsilon)+}$–$Fe^{(2.5+\epsilon)+}$ and $Fe^{(3-\epsilon)+}$–$Fe^{(3-\epsilon)+}$ ($0 < \epsilon < 0.25$) for the α pair and the remaining pair, β, respectively. Mössbauer spectroscopy also elucidates the spin structure of the electronic ground state.[7] Satisfactory fits of the spectra are obtained if it is assumed that the spins of both the α pair (S_{AB}) and the β pair (S_{CD}) are good quantum numbers, which are coupled to resultant total S: $|((S_A,S_B)S_{AB},(S_C,S_D)S_{CD})S\rangle$. For each allowed value of the mixed-valence pair spin, S_{AB}, two values of the ferric pair spin, $S_{CD} = S_{AB} \pm 1/2$, are compatible with the value $S = 1/2$ of the total spin. The effective A values of the ferric pair (β) are found to be *positive*; i.e., of sign opposite that in mononuclear species, so its spin, S_{CD}, must be aligned opposite to the total spin S. In other words, the spin of the mixed-valence pair (α) exceeds the spin of the mixed-valence pair (β) by 1/2: $S_{CD} = S_{AB} - 1/2$. This result also rationalizes the g values with an average slightly greater than 2 observed at the $S = 1/2$ EPR resonance.[7] The preference for the $|(S_{AB},S_{AB} - 1/2)1/2\rangle$ state can be explained by adopting different values for the exchange-coupling constants in the Fe(III)–Fe(III) and Fe(II)–Fe(III) pairs of clusters.[15] Empirical estimates of their values show that the ferric–ferric coupling J_1 is about twice as strong as the ferric–ferrous coupling J: $J_1 = 2J = -350$ cm^{-1},[16] which leads to an energy separation between the levels $|(9/2,4)1/2\rangle$ and $|(9/2,5)1/2\rangle$ of about 440 cm^{-1}.

Concerning the value of the mixed-valence pair spin, S_{AB}, in the ground state of the tetranuclear cluster in oxidized HiPIP, we remark the following. The spin of the corresponding pair in the ground state of related trinuclear $[Fe_3S_4]^0$ cores is equal to 9/2, indicating that the local iron spins therein are aligned parallel.[13] Whence, it is tempting to assume that the same subspin is also present in the mixed-valence pair of oxidized HiPIP, which would imply a ground state of the form $|(9/2,4)1/2\rangle$. We note, however, that even a careful analysis of the Mössbauer data for the effective A values of the $[Fe_4S_4]^{3+}$ core in HiPIP can hardly discern the latter state from the state $|(7/2,3)1/2\rangle$. Lower values of the subspin, $S_{AB} < 7/2$, are, however, clearly incompatible with the magnetic hyperfine data.

The synthesis of $[Fe_4S_4(SR)_4]^{3-/2-}$ model complexes by Holm and co-workers[15,16] made the two lowest oxidation states of the tetranuclear iron–sulfur cores, $[Fe_4S_4]^{+,2+}$, accessible to systematic analysis.[19-21] Initially, similar studies of the highest oxidation state were precluded by the instability of the $[Fe_4S_4(SR)_4]^-$ complex, until the use of sterically encumbered thiolates allowed for the stabilization and isolation of model complexes containing a core $[Fe_4S_4]^{3+}$.[22,23] These complexes display EPR and Mössbauer spectra very similar to those observed in oxidized HiPIP.[24] The four iron sites in the model systems appear again in two different pairs, of which the sets of hyperfine parameters match very well those of the protein. The temperature dependence of the magnetic susceptibility recorded in the same model was analyzed in the framework of an effective Hamiltonian description, including terms for Heisenberg–Dirac–Van Vleck (HDVV) exchange and double exchange in the delocalized pair.[27] The energy level scheme deduced from these data has ground state $|(9/2,4)1/2\rangle$, with a nearly degenerate excited level, $|(7/2,3)1/2\rangle$, lying at 11 cm^{-1}. Single-crystal ENDOR measurements on $[Fe_4S_4]^{3+}$ cores, created by γ irradiation through electron depletion of $[Fe_4S_4]^{2+}$ units in an $[Fe_4S_4(SCH_2C_6D_5)_4][N(C_2D_5)_4]_2$ lattice, give access to detailed information about spin distributions with respect to the crystal frame.[25,26] The method distinguishes electron delocalization over two structurally inequivalent iron pairs present in the depleted cores. Accordingly, the spin-state structures have been interpreted to be $|(9/2,4)1/2\rangle$ and $|(7/2,3)1/2\rangle$.[26]

The similarity of the electron distributions observed in the oxidized HiPIP and in models with chemically equivalent iron sites provides evidence for the hypothesis that the pair delocalization in the ground state of this system is not primarily controlled by protein structure but is rather an *intrinsic* property of the iron–sulfur core. Similar pair delocalization phenomena are observed in triiron units of the form $[Fe_3S_4]^0$ in symmetric model complexes with chemically equivalent sites[28,29] as well as in proteins.[13]

It has been proposed that the electron delocalization properties of the iron–sulfur clusters are a consequence of the conjunction of two physical effects which are inherent to any mixed-valence cluster, viz., electron transfer and vibronic coupling.[30,31] Electron-transfer interactions are of great importance in clusters with equivalent sites, as they may lead to resonances between degenerate, localized valence states. The ensuing electron delocalization gives rise to double-exchange coupling of the local spins in clusters with paramagnetic ions. The concept of double-exchange coupling was introduced by Zener for the explanation of the ferromagnetism in a number of mixed-valence semiconductors[32] and was further developed by several groups in studies of mixed-valence clusters.[33-44] The coupling mechanism results from the marked dependence of the resonance energy on the

(15) Noodleman, L. *Inorg. Chem.* **1988**, *27*, 3677–3679.
(16) Bertrand, P.; Guigliarelli, B.; More, C. *New J. Chem.* **1991**, *15*, 445–454.
(17) Berg, J. M.; Holm, R. H. In *Metal Ions in Biology*; Spiro, T. G., Ed.; Interscience: New York, 1982; Vol. 4, Chapter 1, pp 1–66.
(18) Holm, R. H.; Ciurli, S.; Weigel, J. A. *Prog. Inorg. Chem.* **1990**, *38*, 1–74.
(19) Carney, M. J.; Papaefthymiou, G. C.; Spartalian, K.; Frankel, R. B.; Holm, R. H. *J. Am. Chem. Soc.* **1988**, *110*, 6084–6095.
(20) Carney, M. J.; Papaefthymiou, G. C.; Whitener, M. A.; Spartalian, K.; Frankel, R. B.; Holm, R. H. *Inorg. Chem.* **1988**, *27*, 346–352.
(21) Carney, M. J.; Papaefthymiou, G. C.; Frankel, R. B.; Holm, R. H. *Inorg. Chem.* **1989**, *28*, 1497–1503.
(22) Ueyama, N.; Terakawa, T.; Sugawara, T.; Fuji, M.; Nakamura, A. *Chem. Lett.* **1984**, 1287–1290.
(23) O'Sullivan, T.; Millar, M. M. *J. Am. Chem. Soc.* **1985**, *107*, 4096–4097.
(24) Papaefthymiou, G. C.; Millar, M. M.; Münck, E. *Inorg. Chem.* **1986**, *25*, 3010–3014.
(25) (a) Rius, G.; Lamotte, B. *J. Am. Chem. Soc.* **1989**, *111*, 2464–2469. (b) Gloux, J.; Gloux, P.; Lamotte, B.; Rius, G. *Phys. Rev. Lett.* **1985**, *54*, 599–602.
(26) (a) Mouesca, J. M.; Lamotte, B.; Rius, G. *J. Inorg. Biochem.* **1991**, *43*, 251. (b) Mouesca, J. M.; Rius, G.; Lamotte, B. *J. Am. Chem. Soc.* **1993**, *115*, 4714–4731.
(27) Jordanov, J.; Roth, E. K. H.; Fries, P. H.; Noodleman, L. *Inorg. Chem.* **1990**, *29*, 4288–4292.
(28) (a) Weigel, J. A.; Srivastava, K. K. P.; Day, E. P.; Holm, R. H. *J. Am. Chem. Soc.* **1990**, *112*, 8015–8023. (b) Coucouvanis, D.; Al-Ahmad, S. A.; Salifoglou, A.; Papaefthymiou, V.; Kostikas, A.; Simopoulos, A. *J. Am. Chem. Soc.* **1992**, *114*, 2472–2482.
(29) Mascharak, P. K.; Papaefthymiou, G. C.; Frankel, R. B.; Holm, R. H. *J. Am. Chem. Soc.* **1981**, *103*, 6110–6116.
(30) Girerd, J.-J. *J. Chem. Phys.* **1983**, *79*, 1766–1775.
(31) Borshch, S. A.; Chibotaru, L. F. *Chem. Phys.* **1989**, *135*, 375–380.
(32) Zener, C. *Phys. Rev.* **1951**, *82*, 403–405.
(33) Anderson, P. W.; Hasegawa, H. *Phys. Rev.* **1955**, *100*, 675–681.
(34) Blondin, G.; Girerd, J.-J. *Chem. Rev.* **1990**, *90*, 1359–1376.
(35) Blondin, G.; Borshch, S. A.; Girerd, J.-J. *Comments Inorg. Chem.* **1992**, *12*, 315–340.
(36) Borshch, S. A.; Kotov, I. N.; Bersuker, I. B. *Sov. J. Chem. Phys.* **1985**, *3*, 1009–1016.
(37) Borshch, S. A.; Kotov, I. N.; Bersuker, I. B. *Chem. Phys. Lett.* **1984**, *111*, 264–270.
(38) Belinskii, M. I.; Tsukerblat, B. S.; Gerbeleu, N. V. *Sov. Phys. Solid State (Engl. Transl.)* **1983**, *25*, 497–498.
(39) (a) Belinskii, M. I. *Mol. Phys.* **1987**, *60*, 793–819; (b) *Chem. Phys.* **1993**, *172*, 189–211; (c) *Chem. Phys.* **1993**, *172*, 213–238.
(40) Noodleman, L.; Baerends, E. J. *J. Am. Chem. Soc.* **1984**, *106*, 2316–2327.
(41) Noodleman, L. In *Advances in Inorganic Chemistry*; Sykes, A. G., Ed.; Academic Press: New York, 1992; pp 423–470.
(42) Noodleman, L.; Case, D. A.; Sontum, S. *J. Chim. Phys.* **1989**, *86*, 743–755.
(43) Sontum, S.; Noodleman, L.; Case, D. A. In *The Challenge of d and f Electrons: Theory and Computation*; Salahub, D. R., Zerner, M. C., Eds.; ACS Symposium Series 394; American Chemical Society: Washington, DC, 1989; pp 366–377.
(44) Ding, X. Q.; Bominaar, E. L.; Bill, E.; Winkler, H.; Trautwein, A. X.; Drüeke, S.; Chaudhuri, P.; Wieghardt, K. *J. Chem. Phys.* **1990**, *92*, 178–186.

relative orientation of the core spins at the interacting atoms: the transfer energy is maximum for a parallel alignment of the core spins, but it is reduced by spin-projection factors in the case of tilted spin arrangements.[33] As a consequence, the double-exchange coupling in dimeric units will stabilize an orbitally *non*degenerate ground state of maximum spin in which the excess-electron charge is equally distributed over the two paramagnetic centers. On the contrary, the symmetric tri- and tetranuclear mixed-valent species may possess *degenerate* ground states, including states of different spin and orbital degeneracy, depending on the sign of the electron-transfer parameter, β.[35-39]

Vibronic interactions underlie the electron localization phenomena in symmetric mixed-valence systems.[45,46] The excess electron is vibronically trapped at one site of the cluster by local ligand shell distortions if the set of electronic states is degenerate. Site trapping is thus a property common to all symmetric polynuclear systems displaying weak transfer interactions. For stronger transfer interactions, distortions from ideal symmetry and concomitant (partial) electron localization may arise either by vibronic interaction within an orbitally degenerate state (Jahn–Teller effect) or by vibronic interactions between terms of different energy (pseudo-Jahn–Teller effect).[31,47-52] The former localization phenomena persist in the limit of infinite β values, whereas the distortions approach zero in the latter case. Pseudo-Jahn–Teller distortions are responsible for electron trapping in symmetric mixed-valence dimers. Combinations of Jahn–Teller and pseudo-Jahn–Teller effects are found in symmetric tri- and tetranuclear clusters and are the origin of the nonhomogeneous charge distributions observed therein.

The consideration of spin-dependent localization phenomena in d^5-d^5-d^6 clusters, which follow from the conjunction of spin-dependent electron transfer (double-exchange) and vibronic coupling, allowed us to give a consistent description of both the electron distributions and the spin-state structures observed in the $[Fe_3S_4]^0$ cores of reduced ferredoxin II and its synthetic analogues.[50] The study presented in ref 51 revealed a similar tendency toward pair delocalization in the system d^1-d^1-d^1-d^2, and we now want to extend our approach to the oxidized state of HiPIP and synthetic models thereof.

Description of the Model

Construction of the Electronic Basis States. We consider a four-nuclear cluster of tetrahedral (T_d) symmetry with metal centers A, B, C, and D. The formal oxidation state of the cluster reads d^5-d^5-d^5-d^6. There are five localized 3d-type orbitals at each center: $|a\rangle$, $|a_{1,-,4}\rangle$, $|b\rangle$, $|b_{1,-,4}\rangle$, $|c\rangle$, $|c_{1,-,4}\rangle$, $|d\rangle$, and $|d_{1,-,4}\rangle$. The indexed orbitals are singly occupied. The unindexed orbitals are singly occupied at the three ferric (d^5) sites and doubly occupied at the ferrous (d^6) site. The spins of the unpaired electrons at each center are coupled parallel in order to obey Hund's rule, leading to local spins $S_X^0 = 5/2$ (ferric) and $S_X = 2$ (ferrous), with X = A, B, C, or D. The space of electronic cluster states considered here is spanned by antisymmetrized products of the single-site, high-spin functions. It is convenient to pass to a basis, consisting of eigenfunctions of proper total spin. As we are dealing with a four-spin problem, there exists a considerable freedom in the choice of the spin-coupling scheme in the definition of these electronic basis states. In our numerical analysis of the electron delocalization problem, we adopt the basis

$$\begin{aligned} &|(S_A,((S_B^0,S_C^0)S_{BC}^0,S_D^0)S_{BCD}^0)S\rangle \\ &|(S_B,((S_C^0,S_D^0)S_{CD}^0,S_A^0)S_{ACD}^0)S\rangle \\ &|(S_C,((S_D^0,S_A^0)S_{AD}^0,S_B^0)S_{ADB}^0)S\rangle \\ &|(S_D,((S_A^0,S_B^0)S_{AB}^0,S_C^0)S_{ABC}^0)S\rangle \end{aligned} \quad (1)$$

The notation $(S_k^0,S_l^0)S_{kl}^0$ stands for the standard spin vector coupling of the spins S_k^0 and S_l^0 into resultant spin S_{kl}^0. The basis functions are characterized by the position of the ferrous site, the total spin S which can range from 1/2 to 19/2, and the values of the intermediate spins S_{kl}^0 and S_{klm}^0. The spin quantum numbers are constrained by the usual triangular inequalities: $0 \le S_{kl}^0 \le 5$, $|S_{kl}^0 - 5/2| \le S_{klm}^0 \le S_{kl}^0 + 5/2$, and $|S_{klm}^0 - 2| \le S \le S_{klm}^0 + 2$.

Effective Hamiltonian. Electronic structure calculations of paramagnetic transition-metal clusters starting from the basic electrostatic two-particle interactions and kinetic energy operators face considerable problems of computational nature. Phenomenological approaches are, on the contrary, quite feasible and provide moreover a clear insight into the basic mechanisms underlying the essential features of these systems.

In the present work, the basic interactions are represented by an effective Hamiltonian, $H_{eff} = H_t + H_{HDVV} + H_{ev} + H_{el}$, including terms for electron transfer, Heisenberg–Dirac–Van Vleck exchange, electron–vibrational interaction, and elastic energy of nuclear vibrations, respectively. The initial degeneracy of the electronic basis states (eq 1) is removed by the action of the operator H_{eff}.

The operator H_t is a one-electron operator which transfers electrons between the localized states of the cluster, thereby multiplying the resulting states by transfer parameters. Their values depend on the overlap properties of the orbitals implied in the transfer. Transfer processes involving electrons occupying the indexed orbitals result in states of considerably higher local energies than of those of the basis states given in eq 1 and will be hereupon ignored. Under this restriction, the transfer operator will act only on the electrons in the doubly occupied orbitals a, b, c, or d. Thus, H_t takes the form

$$H_t = \beta P_0 \sum_{i<j} t_{ij} P_0 \quad (2)$$

where the transfer operators, t_{ij}, are defined by the relations

$$t_{ij}|i\rangle = |j\rangle \quad (3)$$

with i and j indicating the orbitals. P_0 is the projector on the spin space of Hund's rule regarding states. As we consider a system of perfect T_d symmetry, the transfer interactions in the equivalent orbital pairs, (a,b), (a,c), ..., (c,d), are described by a single transfer parameter, β.

The calculation of the transfer matrices for the multielectronic states is simplified by adopting a set of basis states in which the excess electron is put in one of the fictitious orbitals a′, b′, c′, or d′. The excess-electron spin, s, is then coupled to the core spin, S_X^0, of the reduced atom: $(S_X^0,s)S_X$ (coupled core-spin representation). In this way, the system is formally represented by an aggregate of four iron cores, each of spin $S^0 = 5/2$, accommodating an itinerant electron in the primed orbitals. It has been shown[50] that the transfer matrix elements in the coupled core-spin representation are linked to those in the original representation (eq 1) by a factor of 6/5. Subsequently, the transfer matrices can be calculated by means of the procedure given in ref 50. The

(45) Piepho, S. B.; Krausz, E. R.; Schatz, P. N. *J. Am. Chem. Soc.* **1978**, *100*, 2996–3005.
(46) Wong, K. Y.; Schatz, P. N. *Prog. Inorg. Chem.* **1981**, *28*, 369–449.
(47) Borshch, S. A.; Kotov, I. N.; Bersuker, I. B. *Chem. Phys. Lett.* **1982**, *89*, 381–384.
(48) Launey, J.-P.; Babonneau, F. *Chem. Phys.* **1982**, *67*, 295–300.
(49) Cannon, R. D.; Montri, L.; Brown, D. B.; Marshall, K. M.; Elliott, M. C. *J. Am. Chem. Soc.* **1984**, *106*, 2591–2594.
(50) Borshch, S. A.; Bominaar, E. L.; Blondin, G.; Girerd, J.-J. *J. Am. Chem. Soc.* **1993**, *115*, 5155–5168.
(51) Borshch, S. A.; Bominaar, E. L.; Girerd, J.-J. *New J. Chem.* **1993**, *17*, 39–42.
(52) Marks, A. J.; Prassides, K. *J. Chem. Phys.* **1993**, *98*, 4805–4813. For the solution of the vibronic problem of one electron on a tetrahedron, see also: Marks, A. J.; Prassides, K. *New J. Chem.* **1993**, *17*, 59–65.

Table 1. Energy Eigenvalues of the Tetrahedral d^5-d^5-d^5-d^6 Double-Exchange Problem

spin	energy/β (degeneracy)			total no.
19/2	3 (1)	−1 (3)		4
17/2	14/5 (3)	−4/5 (6)	−6/5 (3)	12
15/2	13/5 (6)	−3/5 (10)	−6/5 (8)	24
13/2	12/5 (10)	−2/5 (15)	−6/5 (15)	40
11/2	11/5 (15)	−1/5 (21)	−6/5 (24)	60
9/2	2 (21)	0 (24)	−6/5 (35)	80
7/2	9/5 (24)	1/5 (24)	−6/5 (40)	88
5/2	8/5 (24)	2/5 (21)	−6/5 (39)	84
3/2	7/5 (21)	3/5 (15)	−6/5 (32)	68
1/2	6/5 (15)	4/5 (6)	−6/5 (19)	40

eigenvalues of the transfer matrices dependent on the total spin are given in Table 1 (see also ref 53).

The Heisenberg–Dirac–Van Vleck (HDVV) operator in T_d symmetry, describing the intercenter exchange interactions, reads

$$H_{\mathrm{HDVV}} = -\sum_{i,j,k,l}[JS_i(S_k + S_l + S_m) + J_1(S_kS_l + S_kS_m + S_lS_m)]n_i \quad (4)$$

where the summation is over the labels i,k,l,m = ABCD, DABC, CDAB, and BCDA. The HDVV Hamiltonian given in eq 4 accounts for the different values of the exchange-coupling constants in ferrous–ferric (J) and ferric–ferric (J_1) pathways. The occupation number operator n_i (i = A,B,C,D) keeps track of the center containing the excess electron, i.e., $n_i = 1$ if the electron is at site i and 0 otherwise. The HDVV operator given in eq 4 is diagonal in the localized representation defined by eq 1. The diagonal elements are given by the expression

$$E(S,S_{klm}{}^0) = E^0 - JS(S+1)/2 - (J_1 - J)S_{klm}{}^0(S_{klm}{}^0 + 1)/2 \quad (5)$$

where E^0 is a constant term common to all spin-state energies.

The relaxation of the ligand shell upon addition of the excess electron in a localized state is accounted for by the electron–vibrational interaction term

$$H_{\mathrm{ev}} = \sum_i \lambda Q_i n_i \qquad i = \mathrm{A,B,C,D} \quad (6)$$

where λ is the vibronic coupling parameter independent of spin, coordinate Q_i measures a symmetric local distortion around center i, and n_i is its electronic occupation operator. We pass, for convenience, to symmetrized coordinates, which for a tetrahedral system read

$$\begin{aligned} Q_a &= (\mathrm{Q_A} + \mathrm{Q_B} + \mathrm{Q_C} + \mathrm{Q_D})/2 \\ Q_x &= (\mathrm{Q_A} + \mathrm{Q_B} - \mathrm{Q_C} - \mathrm{Q_D})/2 \\ Q_y &= (\mathrm{Q_A} - \mathrm{Q_B} - \mathrm{Q_C} + \mathrm{Q_D})/2 \\ Q_z &= (\mathrm{Q_A} - \mathrm{Q_B} + \mathrm{Q_C} - \mathrm{Q_D})/2 \end{aligned} \quad (7)$$

and transform according to the representations a_1 (Q_a) and t_2 (Q_x, Q_y, Q_z) of the tetrahedral group. The origin in Q space corresponds to a structure of perfect T_d symmetry, which is depicted by four shells of equal radii at the bottom left of Figure 2. Points off the origin represent structures of symmetry lower than T_d. The points on the cube in Figure 2 define some selected directions in which the distortions represent lower symmetries: three-fold symmetry (A, B, .., ABC, ...) and two-fold symmetry (AB, AC, ...). The size of the distortion is, in each direction, proportional to the distance to the origin. H_{ev} can be expressed

(53) Borras-Almenar, J. J.; Coronado, E.; Georges, R.; Gomez-Garcia, C. J. *Chem. Phys.* **1992**, *166*, 139–144.

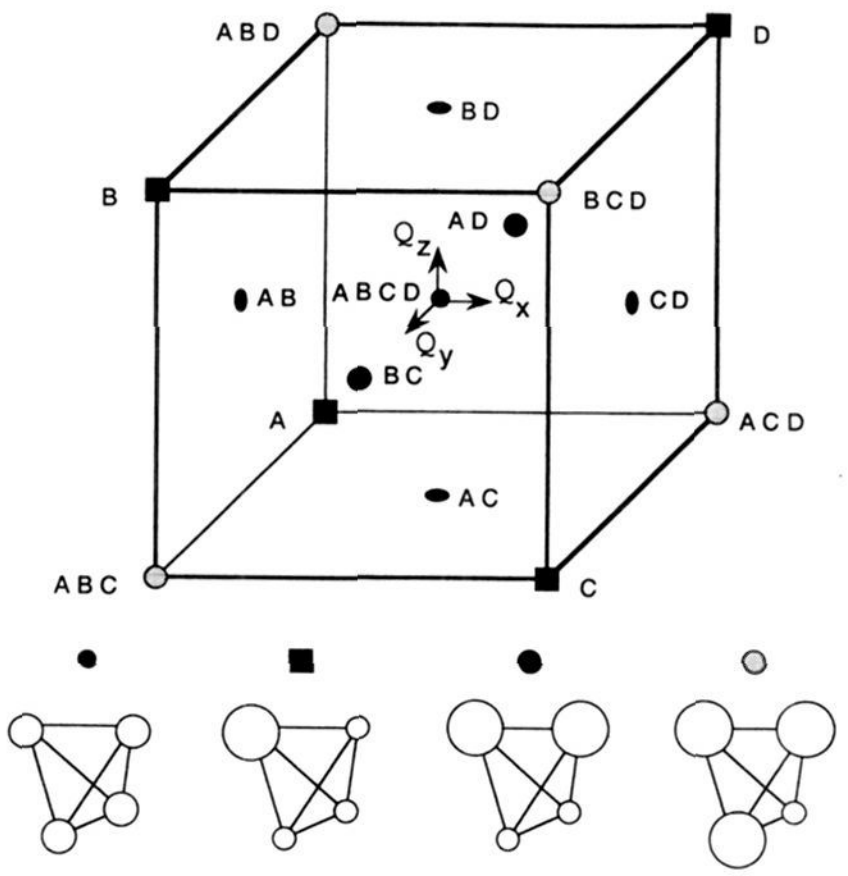

Figure 2. Space of symmetrized vibrational coordinates, Q_x, Q_y, and Q_z. The labels, A, ..., AB, ..., ABC, ..., and ABCD mark directions with one, two, three, and four dilated ligand shells, leading to electron delocalization over monomeric, dimeric, trimeric, and tetrameric subunits of the cluster, respectively.

in the symmetrized coordinates as

$$\begin{aligned} H_{\mathrm{ev}} &= \lambda[Q_a/2 + Q_x(n_\mathrm{A} + n_\mathrm{B} - n_\mathrm{C} - n_\mathrm{D})/2 + Q_y(n_\mathrm{A} - n_\mathrm{B} - n_\mathrm{C} + n_\mathrm{D})/2 + Q_z(n_\mathrm{A} - n_\mathrm{B} + n_\mathrm{C} - n_\mathrm{D})/2] \\ &= \lambda[Q_a/2 + n_xQ_x + n_yQ_y + n_zQ_z] \end{aligned} \quad (8)$$

The interaction with vibration Q_a is identical for all electronic states and can be ignored.

Finally, the sum of the elastic energies of the symmetric local vibrations around the four metal centers,

$$H_{\mathrm{el}} = (\kappa/2)\sum_i Q_i^2 = (\kappa/2)(Q_a{}^2 + Q_x{}^2 + Q_y{}^2 + Q_z{}^2) \qquad i = \mathrm{A,B,C,D} \quad (9)$$

(Q_a is taken to be zero hereafter), is added. The factor κ in eq 9 is the force constant of the iron–sulfur bond, which is assumed to be independent of oxidation state.

The diagonalization of the interaction matrices of the total Hamiltonian H_{eff} yields the electronic energies as a function of the coordinates Q_x, Q_y, and Q_z. The adiabatic energy surfaces thus obtained for different spins can be numerically studied. The lowest minima of the adiabatic surfaces define, in semiclassical approximation, the spin, the stable nuclear configuration, and the electron distribution of the ground state. The numerical results for these properties will be analyzed in the next section.

Results and Discussion

Electron Distribution and Spin in the Ground State. The tetrahedral symmetry of the Hamiltonian H_{eff} imposes the same symmetry on the adiabatic potential surfaces defined on the vibrational space. The adiabatic potential surfaces are independent of spin in the absence of transfer interaction ($\beta = 0$) and of HDVV exchange ($J = J_1 = 0$), so they are forming multi-spin-degenerate sheets in those cases. The lowest sheet possesses four equivalent absolute minima along the trigonal directions in Q space, (−1,−1,−1), (−1,1,1), (1,1,−1), and (1,−1,1), pointing toward the vertices of the tetrahedron shown in Figure 2. In each of these directions, indicated in Figure 2 by A, B, C, and D,

respectively, three of the coordination spheres are equally contracted and the remaining one is dilated. The excess electron in the minima is localized at the center in the dilated ligand shell. The vibronic energy gained by the site trapping of the electron is equal to $\lambda^2/2\kappa$. There are furthermore two types of saddle points on the potential surfaces. Four equivalent saddle points are located along the directions (1,1,1), (−1,−1,1), (−1,1,−1), and (1,−1,−1), i.e., in the directions opposite those of the minima. Accordingly, the excess electron is delocalized over three dilated sites, which are indicated in Figure 2 by the labels BCD, ABD, ABC, and ACD, respectively. Another set of equivalent saddle points is situated along the directions (1,0,0), (−1,0,0), (0,1,0), (0,−1,0), and (0,0,1), and (0,0,−1). They are associated with excess-electron delocalization over the six dilated pairs CD, AB, BC, AD, BD, and AC, respectively (Figure 2), and lie halfway between the two corresponding minima. The latter saddle points correspond to minima in the sections of the lowest potential well along the Q_i axes and are located a distance of $\lambda/2\kappa$ from the origin. A representative set of minima and saddle points can be discerned on the adiabatic surface defined on the diagonal planes of the cube in Q space, which is depicted in Figure 3A. The surfaces in the figure were constructed, for computational convenience, for a smaller system, d^1-d^1-d^1-d^2, which exhibits the same qualitative features as those of the genuine system, d^5-d^5-d^5-d^6.

It can be seen from Table 1 that the electronic ground state of the transfer operator H_t in the system d^5-d^5-d^5-d^6 essentially depends on the sign of the transfer parameter β. For negative values of β, there exists an orbitally nondegenerate ground state of maximum spin, $S = 19/2$, which is separated by an energy gap of $\beta/5$ from the first excited state. The excess electron in this ground state is equally distributed over the four sites of the tetramer. Since the transfer interactions in the high-spin state are not weakened by spin-projection factors, as is the case for lower spin numbers, the high-spin state becomes the ground state. The same type of double-exchange-stabilized, high-spin ground states can be derived for $\beta < 0$ in the theory of mixed-valence dimers and trimers. For positive values of β, the ground state of the electronic hamiltonian, H_t, is 215-fold degenerate, including states of spins ranging from 1/2 to 17/2. Moreover, the ground manifolds of spin S are orbitally degenerate for each spin number $1/2 \le S \le 17/2$.

The values of β as obtained by quantum chemical computations on iron–sulfur clusters are found to differ in sign and magnitude.[41,50] The contradictions about the sign of the effective β values may owe to the preponderance of one or the other of the antagonistic contributions to β deriving from the various "through-bond" and "through-space" pathways, depending on the computational method used. Experimental data on transfer parameter values in iron–sulfur clusters are as yet not available. In view of the lack of unanimity as to this number, we shall consider the full β range including negative and positive values.

For small, negative values of β ($|\beta|/(\lambda^2/2\kappa) \ll 1$), the positions of the minima in Q space are, obviously, close to those found for $\beta = 0$. The excess electron, although still mainly localized at one site, is then also slightly delocalized toward the other sites of the system. These transfer interactions, which depend on spin, remove the degeneracy of the spin-state energies and give rise to an effective ferromagnetic coupling of the local spins, leading to the energy order $E(19/2) < E(17/2) < \ldots < E(1/2)$. The energy intervals between the spin-multiplet energies obey the Landé rule for sufficiently small values of β. The same property can be derived for dimers[30] and trimers.[35] The positions of the energy minima in Q space are drastically changed by increasing β further in magnitude. The energy order of the spin states, however, which is imposed by the transfer interaction (see Table 1), remains unchanged. The energy of the orbitally nondegenerate electronic $S = 19/2$ ground state is well separated from the other $S = 19/2$ levels for strong, negative transfer interaction, $\beta/(\lambda^2/2\kappa) < -1$, so pseudo-Jahn–Teller distortions become negligible. Consequently, the minimum of the lowest adiabatic surface is located at the origin in Q space. The electron-transfer interaction in tetrameric units thus results in the stabilization of a completely delocalized ground state of maximum spin for negative β values of sufficient magnitude, just like in dimers[30] and trimers.[35,50]

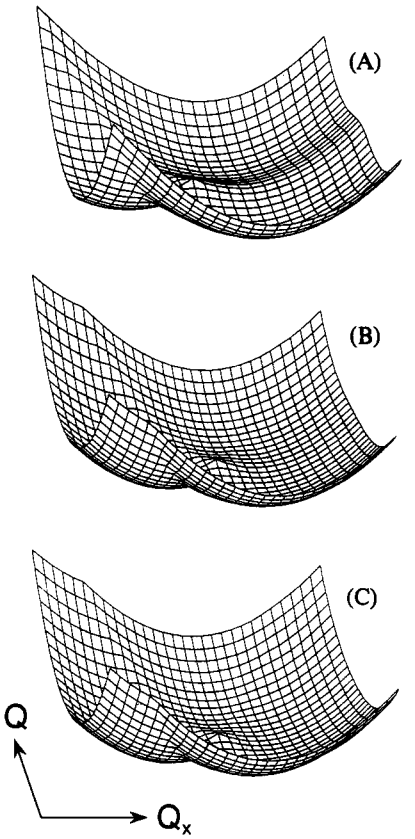

Figure 3. Adiabatic potential surfaces for the $S = 1/2$ state of the model system d^1-d^1-d^1-d^2 in the plane $Q_y + Q_z = 0$, depicting the minima and saddle points discussed in the text. Parameters used: $\kappa = 1$, $\lambda = 2$, $\beta =$ 1 (A), 3 (B), and 7 (C). The two equivalent minima in A are located in the directions with site localization indicated by C and D in Figure 2. The two minima in C have merged into a single minimum located in the direction CD for pair delocalization.

For small, positive values of β, we have again predominant excess-electron localization at one center for all spin states. These states are split in the same energy order as in the case of negative β values, due to slight spin-dependent electron delocalizations. Systems with positive β values behave, however, completely differently from those with negative β values in the domain of strong transfer interaction. The orbitally degenerate ground states of spin $S = 1/2, \ldots, 17/2$, found for $\beta > 0$ (see Table 1), lead to Jahn–Teller distortions which persist in the limit $\beta/(\lambda^2/2\kappa) \gg 1$. For ratios greater than 1, the minima of the lowest adiabatic surface for the spin $S = 1/2$ are located at six equivalent positions on the Q_i axes. These minima correspond to the second set of saddle points obtained before for $\beta \approx 0$ (see Figure 3). The corresponding structures have two-fold symmetry and contain two contracted and two dilated ligand spheres which are labeled by AB, ... in Figure 2. The expanded spheres contain the major part of the excess-electron charge, which is equally distributed over the two centers inside them; the remaining electron charge is equally distributed over the two contracted sites. In other words, the electron distribution reflects the symmetry of the distorted structures at the minima. The order of the spin-state energies calculated for large, positive β values does not simply proceed, as for negative β values, for the energy spectrum of the transfer operator H_t, due to the degeneracy of the electronic ground

state (see Table 1). Numerical analysis reveals that the degeneracy of the ground-state energies is removed by the action of the vibronic interaction. The broken-symmetry $S = 1/2$ state becomes the ground state for $\beta/(\lambda^2/2\kappa) > 1.1$. The energies of the spin ground levels appear as $E(1/2) < E(3/2) < ... < E(17/2)$ for $\beta/(\lambda^2/2\kappa) > 3$, which is the opposite order of that obtained for small β values. Minima located at the Q_i axes are also obtained for $S = 3/2, 5/2, 7/2$, and $9/2$. For these and higher spin numbers, there may exist, however, depending on the value of β, energetically close-lying local minima in different nonequivalent directions. The coordinates of the axial minima appear, for $\beta/(\lambda^2/2\kappa) > 3$, in the order $\lambda/2\kappa > Q_i(1/2) > Q_i(3/2) > ... > Q_i(g/2)$. It follows that the excess electron in the minima is not strictly confined to the dilated pairs, but it has also a nonvanishing probability density, increasing with spin S, to be found at two contracted centers. We notice, however, that the vibronic energy splittings between the spin multiplet energies are rather small. By adopting a vibronic site trapping energy of $\lambda^2/2\kappa = 2000$ cm^{-1} and $\beta/(\lambda^2/k) = 3$, we find the energy splittings $E(3/2)$–$E(1/2)$ and $E(17/2)$–$E(1/2)$ to amount to 3 and 194 cm^{-1}, respectively.

The pair delocalization and the spin quantum number, $S = 1/2$, in the orbitally nondegenerate ground state of the Hamiltonian $H_t + H_{ev}$ agree with the empirical results for these properties in oxidized HiPIP and related model complexes. The spin-state structure of the broken-symmetry, "pair"-delocalized, $S = 1/2$ ground state will be analyzed in the next section.

Spin Structure of the Broken-Symmetry, $S = 1/2$ Ground State. The spectroscopic investigations of oxidized HiPIP and its synthetic analogues show that the spin quantum number of the ground state is $S = 1/2$ and provide also detailed information on the coupling pattern of the local spins (see Introduction). In the following, we examine the spin structures of the broken-symmetry states obtained by our model in the limit of strong transfer interaction, $\beta/(\lambda^2/2\kappa) \gg 1$.

The analysis is facilitated by employing an electronic basis which is adapted to the two-fold symmetry of the distorted structures. The axis Q_x is thereby taken as the priviliged direction. We introduce first a convenient basis for the electronic functions of the dinuclear fragments AB and CD of the tetramer. The functions for the pair containing the excess electron (e.g., AB) are defined as the eigenstates of the transfer operator in the dimer. These states formally correspond to the expressions[50]

$$\Phi_{\pm}{}^{S}{}_{AB} = (1/\sqrt{2})[|((S_A{}^0,s)S_A,S_B{}^0)S_{AB};a'\rangle \mp |(S_A{}^0,(s,S_B{}^0)S_B)S_{AB};b'\rangle] \quad (10a)$$

Then, by adopting a coupling scheme in which the composite core spin, $S_{AB}{}^0$, is coupled to the excess-electron spin s, eq 10a takes the form[50]

$$\Phi_{\pm}{}^{S}{}_{AB} = [(2S^0 + S_{AB} + 3/2)/(4S^0 + 2)]^{1/2}|((S_A{}^0,S_B{}^0)S_{AB}{}^0 = S_{AB} + 1/2,s)S_{AB};\phi_{\pm}{}^{AB}\rangle + [(2S^0 - S_{AB} + 1/2)/(4S^0 + 2)]^{1/2}|((S_A{}^0,S_B{}^0)S_{AB}{}^0 = S_{AB} - 1/2,s)S_{AB};\phi_{\mp}{}^{AB}\rangle \quad (10b)$$

The excess electron in this expression is described by the pair-delocalized orbitals

$$\phi_{\pm}{}^{AB} = (|a'\rangle \pm |b'\rangle)/\sqrt{2} \quad (11)$$

The transfer energies of the dimer states are given by the expression

$$E_{\pm}{}^{S_{AB}} = \pm\beta(S_{AB} + 1/2)/2S^0 \quad (12)$$

where $S^0 = 5/2$, and the upper and lower sign correspond to those in eq 10. The electronic functions of the pair without excess electron (e.g., CD) are defined by straightforward spin coupling as

$$|S_{CD}{}^0\rangle = |(S_C{}^0,S_D{}^0)S_{CD}{}^0\rangle \quad (13)$$

A set of symmetry-adapted, formal basis states for the tetramer is defined by spin coupling of the fragment functions:

$$|(S_{AB},S_{CD}{}^0)S\rangle^{\pm} = |(\Phi_{\pm}{}^{S_{AB}},S_{CD}{}^0)S\rangle = [(2S^0 + S_{AB} + 3/2)/(4S^0 + 2)]^{1/2}[((S_{AB}{}^0 = S_{AB} + 1/2,s)S_{AB},S_{CD}{}^0)S;\phi_{\pm}{}^{AB}\rangle + [(2S^0 - S_{AB} + 1/2)/(4S^0 + 2)]^{1/2}[((S_{AB}{}^0 = S_{AB} - 1/2,s)S_{AB},S_{CD}{}^0)S;\phi_{\mp}{}^{AB}\rangle \quad (14a)$$

in which the excess electron is delocalized over the centers A and B, and

$$|(S_{AB}{}^0,S_{CD})S\rangle^{\pm} = |(S_{AB}{}^0,\Phi_{\pm}{}^{S_{CD}})S\rangle = -[(2S^0 + S_{CD} + 3/2)/(4S^0 + 2)]^{1/2}|(S_{AB}{}^0,(s,S_{CD}{}^0 = S_{CD} + 1/2)S_{CD})S;\phi_{\pm}{}^{CD}\rangle + [(2S^0 - S_{CD} + 1/2)/(4S^0 + 2)]^{1/2}|(S_{AB}{}^0,(s,S_{CD}{}^0 = S_{CD} - 1/2)S_{CD})S;\phi_{\mp}{}^{CD}\rangle \quad (14b)$$

in which the excess electron is delocalized over the centers C and D.

The Hamiltonian matrices of the transfer operator have in symmetry-adapted representation (eq 14a,b) a block-diagonal form, including submatrices of dimensions ≤4 (see Appendix). A representative example of a block matrix for $S = 1/2$ is given in eq 15:

$$\begin{array}{cccc|l} -\beta & (1/45)\beta & 0 & -(4(\sqrt{2})/9)\beta & |(9/2,4)1/2\rangle^- \\ (1/45)\beta & -\beta & (4(\sqrt{2})/9)\beta & 0 & |(4,9/2)1/2\rangle^- \\ 0 & (4(\sqrt{2})/9)\beta & (4/5)\beta & (2/9)\beta & |(7/2,4)1/2\rangle^+ \\ -(4(\sqrt{2})/9)\beta & 0 & (2/9)\beta & (4/5)\beta & |(4,7/2)1/2\rangle^+ \end{array} \quad (15)$$

The diagonalization can be performed analytically by passing first to the basis

$$(|(9/2,4)1/2\rangle^- \pm |(4,9/2)1/2\rangle^-)/\sqrt{2}$$

$$(|(7/2,4)1/2\rangle^+ \pm |(4,7/2)1/2\rangle^+)/\sqrt{2} \quad (16)$$

leading to a decomposition into two 2×2 matrices with eigenvalues $-(6/5)\beta$ (twice), $(4/5)\beta$, and $(6/5)\beta$. The additional interpair interactions enhance the delocalization energy in the ground state by $-\beta/5$. The ground states are given by

$$|\Psi_1\rangle = (2(\sqrt{2})/3)[|(9/2,4)1/2\rangle^- + |(4,9/2)1/2\rangle]^-/\sqrt{2} - (1/3)[|(7/2,4)1/2\rangle^+ - |(4,7/2)1/2\rangle^+]/\sqrt{2} \quad (17)$$

$$|\Psi_2\rangle = (5(\sqrt{3})/9)[|(9/2,4)1/2\rangle^- - |(4,9/2)1/2\rangle^-]/\sqrt{2} + ((\sqrt{6})/9)[|(7/2,4)1/2\rangle^+ + |(4,7/2)1/2\rangle^+]/\sqrt{2}$$

The vibronic coupling operator on the Q_x axis, which reads

$$H_{ev}{}^x = \lambda n_x Q_x = \lambda(n_{AB} - n_{CD})Q_x/2 \quad (18)$$

with $n_{AB} = n_A + n_B$ and $n_{CD} = n_C + n_D$, is diagonal in the symmetry-adapted basis eq 14a,b. The diagonal elements of $H_{ev}{}^x$ in the pair-delocalized states, which must be added to the diagonal energies in eq 15, are given by

$$\langle H_{ev}{}^x\rangle = \pm\lambda Q_x/2 \quad (19)$$

where the + and – signs refer to states in which the excess electron is predominantly delocalized over AB and CD, respectively. As we are considering the case of strong transfer interaction ($\beta/(\lambda^2/2\kappa) \gg 1$), it is convenient to transform the interaction matrices of $H_t + H_{ev}{}^x$ to the eigenfunction basis of H_t. The transformation yields, within the orbitally degenerate ground doublet given in eq 17, the matrix

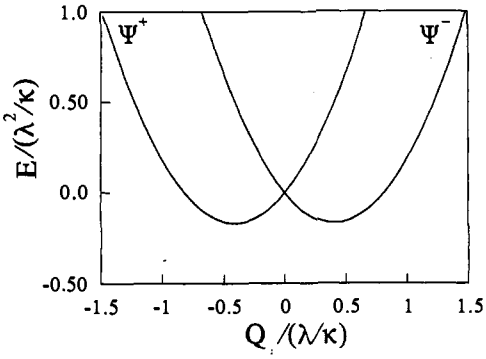

Figure 4. Sum of vibronic and elastic energies of the states Ψ^+ and Ψ^- as a function of Q_x ($Q_y = Q_z = 0$).

$$\begin{array}{lll} -(6/5)\beta & (\lambda/\sqrt{6})Q_x & |\Psi_1\rangle \\ (\lambda/\sqrt{6})Q_x & -(6/5)\beta & |\Psi_2\rangle \end{array} \quad (20)$$

There are also nonvanishing vibronic couplings between the ground states and the excited levels at $(4/5)\beta$ and $(6/5)\beta$. These interactions, however, can be ignored in the limit of strong electron transfer considered here. Diagonalization of eq 20 results in the eigenstates

$$\Psi^{\pm} = (|\Psi_1\rangle \pm |\Psi_2\rangle)/\sqrt{2} \quad (21)$$

which are independent of the values for λ and Q_x. The excess electron in these states is not strictly confined to one of the pairs, AB or CD; the pair spins are not good quantum numbers anymore. The eigenstates in eq 21 optimize the occupation numbers of the pairs AB and CD. This can be seen as follows. The pair occupation numbers in the general doublet state,

$$\Psi(\theta) = \cos\theta\,|\Psi_1\rangle + \sin\theta\,|\Psi_2\rangle \quad (22)$$

are given by the expressions

$$\langle\Psi(\theta)|n_{AB}|\Psi(\theta)\rangle = 1/2 + (1/6)^{1/2}\sin 2\theta \quad (23a)$$

$$\langle\Psi(\theta)|n_{CD}|\Psi(\theta)\rangle = 1/2 - (1/6)^{1/2}\sin 2\theta \quad (23b)$$

Hence, the maximum values for the occupation numbers of AB and CD are attained for the angles $\theta = \pi/4$ and $\theta = -\pi/4$, respectively. Substitution of these values in eq 22 yields indeed the eigenfunctions given in eq 21. The vibronic energies obtained by the diagonalization of eq 20 (or, alternatively, by substitution of the optimal occupation numbers into eq 18) read

$$\langle\Psi^{\pm}|H_{ev}{}^{x}|\Psi^{\pm}\rangle = \pm\lambda(1/6)^{1/2}Q_x \quad (24)$$

The total energy of the eigenstates $\Psi^{\pm}$ along the Q_x axis can be expressed as

$$\langle\Psi^{\pm}|H_t + H_{ev}{}^{x} + H_{el}|\Psi^{\pm}\rangle = -(6/5)\beta \pm \lambda(1/6)^{1/2}Q_x + (\kappa/2)Q_x{}^2 \quad (25)$$

(see Figure 4). The energy minima are reached at

$$Q_x = Q_x{}^0 = -(1/6)^{1/2}\lambda/\kappa \quad (26a)$$

in the Ψ^+ state and at

$$Q_x = -Q_x{}^0 = (1/6)^{1/2}\lambda/\kappa \quad (26b)$$

in the Ψ^- state. The two equivalent minima correspond to predominant excess-electron delocalization over AB and CD, respectively, but as was stated before, the excess electron in the $\Psi^{\pm}$ states is also slightly delocalized toward the other pair of the cluster (see, e.g., eq 23). The occupation number of the minority pair is a function, given in eq 27, of the position coordinate at the energy minimum:

Table 2. Multiplicity of Minima, Average Occupation Number of Minority Pair ($\langle n_{CD}\rangle$), Vibronic Coupling Coefficient ($\langle {}^1/_2 - n_{CD}\rangle$), and Vibronic Stabilization Energy of the 19 Lowest-Energy, Broken-Symmetry, $S = 1/2$ Eigenstates

eigenstate	multiplicity	$\langle n_{CD}\rangle$	$\langle {}^1/_2 - n_{CD}\rangle$	E_{vc}	
$\|(9/2,5)\,1/2\rangle^{-a}$	2[b]	0.0833	5/12	−25/144[c]	−347[d]
$\|(9/2,4)\,1/2\rangle^-$	2	0.0918	$1/\sqrt{6}$	−1/6	−333
$\|(7/2,4)\,1/2\rangle^-$	2	0.1667	1/3	−1/9	−222
$\|(7/2,3)\,1/2\rangle^-$	2	0.1838	$1/\sqrt{10}$	−1/10	−200
$\|(5/2,3)\,1/2\rangle^-$	2	0.2500	1/4	−1/16	−125
$\|(5/2,2)\,1/2\rangle^-$	2	0.2764	$1/\sqrt{20}$	−1/20	−100
$\|(3/2,2)\,1/2\rangle^-$	2	0.3333	1/6	−1/36	−56
$\|(3/2,1)\,1/2\rangle^-$	2	0.3709	$1/\sqrt{60}$	−1/60	−33
$\|(1/2,1)\,1/2\rangle^-$	2	0.4167	1/12	−1/144	−14
$\|(1/2,0)\,1/2\rangle^-$	1	0.5000	0	0	0

[a] Principal component of eigenstate in symmetry-adapted representation. [b] Number of equivalent minima on each Q_i axis. [c] Energies in units $\lambda^2/2\kappa$. [d] Energies in wavenumbers obtained for $\lambda^2/2\kappa = 2000$ cm^{-1}.

$$\langle n_{CD}\rangle = 1/2 - |Q_x{}^0/(\lambda/\kappa)| \quad (27)$$

The energy at the minima, in total six, is given by

$$E^0 = -(6/5)\beta - (1/6)(\lambda^2/2\kappa) \quad (28)$$

where the latter term represents the vibronic stabilization energy.

Interaction matrices of dimension 4×4, similar to that given in eq 15, can be constructed in the function sets $\{|(7/2,3)1/2\rangle^-, |(3,7/2)1/2\rangle^-, |(5/2,3)1/2\rangle^+, |(3,5/2)1/2\rangle^+\}, \{|(5/2,2)1/2\rangle^-, ...\}$, ... For each subset, we can derive, as before, eigenstates with predominant pair delocalization (see eq 21), corresponding to minima located at the Q_i axes at the positive and negative side of the origin (see eq 26). The transfer interaction in the degenerate subset $\{|(1/2,0)1/2\rangle^-, |(0,1/2)1/2\rangle^-\}$ results in electronic states which are completely delocalized over the cluster, having a single minimum located at the origin of Q space. Furthermore, there exist nondiagonal transfer interactions within the following binary subsets: $\{|(9/2,5)1/2\rangle^-, |(4,9/2)1/2\rangle^+\}$, $\{|(9/2,4)1/2\rangle^+, |(5,9/2)1/2\rangle^-\}$, $\{|(7/2,4)1/2\rangle^-, |(3,7/2)1/2\rangle^+\}$, ... The transfer interaction stabilizes, in each of these function sets, an eigenstate of energy $-(6/5)\beta$, in which the excess electron is once more mainly occupying one of the pairs. Altogether, the Hamiltonian matrix of the transfer operator H_t in the space of symmetry-adapted basis functions (eq 14a,b) of spin $S = 1/2$ is block-diagonalized into four 4×4 and twelve 2×2 interaction matrices. Diagonalization yields, among others, 19 eigenstates of energy $-(6/5)\beta$, which are designated in Table 2 by their principal components in symmetry-adapted representation (column 1). The table contains furthermore the number of equivalent minima on each Q_i axis (column 2), the occupation number of the minority pair (column 3), the vibronic coupling coefficient $\langle 1/2 - n_{CD}\rangle$ (column 4), the vibronic stabilization energies at the minima in units of the site trapping energy $\lambda^2/2\kappa$ (column 5, and the latter energies as obtained by adopting a value for $\lambda^2/2\kappa$ (=2000 cm^{-1}) typical for iron–sulfur clusters[50] (column 6). The table reveals the existence of two low-lying, nearly degenerate states with the principal components $|(9/2,5)1/2\rangle^-$ and $|(9/2,4)1/2\rangle^-$ and a series of excited states which appear in the order $|(7/2,4)1/2\rangle^-$, $|(7/2,3)1/2\rangle^-$, $|(5/2,3)1/2\rangle^-$, $|(5/2,2)1/2\rangle^-$, ..., $|(1/2,0)1/2\rangle^-$. The energy order can be qualitatively understood as follows. The *intra*pair delocalization energies within the principal components, $|(S_{AB},S_{AB} \pm 1/2)1/2\rangle^-$, of the eigenstates increase with subspin S_{AB} (see eq 12). As a consequence, the *inter*pair interaction has to decrease simultaneously, in order to maintain the total delocalization energy $-(6/5)\beta$ (see Figure 5). Whence, the excess electron is less smeared out for higher values of S_{AB}, leading to smaller values of $\langle n_{CD}\rangle$ and to higher vibronic stabilization energies. The interpretation of the energy order $|(S_{AB},S_{AB} + 1/2)1/2\rangle^-$ below $|(S_{AB},S_{AB} - 1/2)1/2\rangle^-$ is a more intricate matter which can be settled by straightforward calculation.

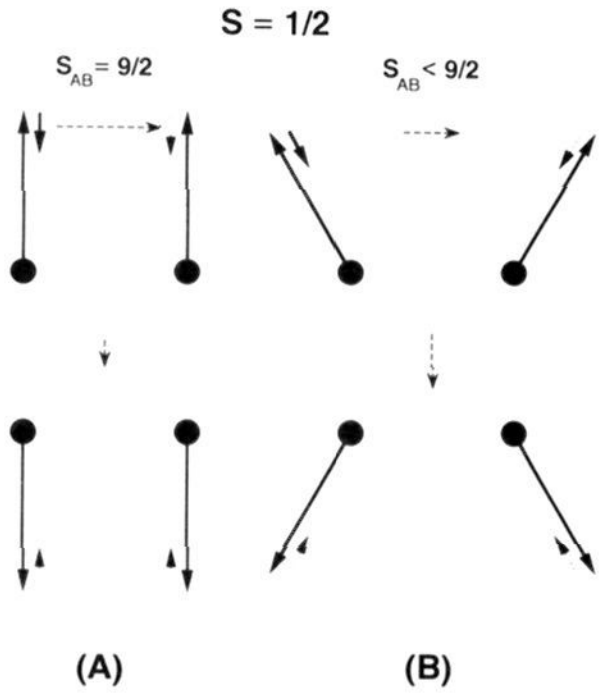

Figure 5. Schematic representation of the strengths of the electron-transfer interactions (broken arrows) in $|(S_{AB} = 9/2, S_{CD}{}^0 = 5)S = 1/2\rangle^{\pm}$ (A) and in a $S = 1/2$ configuration with lower pair-spin numbers: $S_{AB} < 9/2$ and $S_{CD}{}^0 < 5$ (B). Notice that the tiltings of the core spins in B lead to a weaker *intra*dimer interaction but to a stronger *inter*dimer interaction. Consequently, the excess-electron charge in B is more uniformly distributed than that in A.

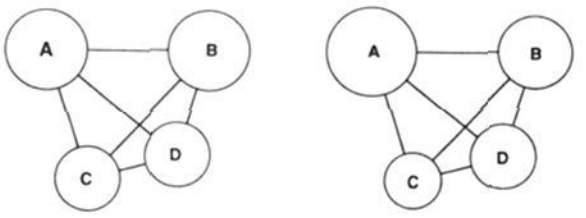

Figure 6. (A) Ligand shell distortions accompanying the pair delocalization phenomenon obtained for $\beta/(\lambda^2/2\kappa) \geq 1$. (B) Ligand shell distortions associated with a point off the Q_x axis, showing the symmetry breaking of the delocalized pair.

The study of the model system d^1-d^1-d^1-d^2, given in ref 51, shows that the excess electron in the ground state of spin $S = 1/2$ therein is strictly confined to a pair of sites for large, positive values of β, whereas in the system d^5-d^5-d^5-d^6, also *inter*pair delocalizations arise, which have, as is documented in Table 2, a significant impact on the spin-state energies. The additional transfer interactions in the latter system are a consequence of the antiparallel alignment of the excess-electron spin relative to the spin of the d^5 core of the atom containing the electron.

The electronic structures, outlined above, of the states "prepared" by the double-exchange interaction underlie, evidently, the stability of the two-fold symmetric ligand shell distortions (Figure 6A) located at Q_i axes. Deviations from the Q_i axes, as illustrated in Figure 6B, break the symmetry of the ligand shell pair, AB, containing the excess electron, in all directions ($Q_x{}^0$, dQ_y, dQ_z) with $dQ_y + dQ_z \neq 0$ (see eq 7). These distortions give rise to vibronic interactions between the pair-delocalized ground state and the excited levels obtained in two-fold symmetry. Like in dimeric mixed-valence units,[45,46] these vibronic interactions have the potential to localize the excess electron at one of the sites A or B. However, for sufficiently large values of the ratio $\beta/(\lambda^2/2\kappa)$, i.e., ≥ 1 in d^5-d^5-d^5-d^6, this localizing interaction is too weak to break the two-fold symmetry. Numerical analysis shows furthermore that the system is also stable to distortions in the direction with $dQ_y + dQ_z = 0$, so we are dealing with a minimum and not with a saddle point.

HDVV Exchange. In this section, we analyze the effect of the interion exchange interactions on the electronic states and their energies as obtained at the adiabatic potential minima. The couplings are described by the HDVV Hamiltonian, eq 4, and

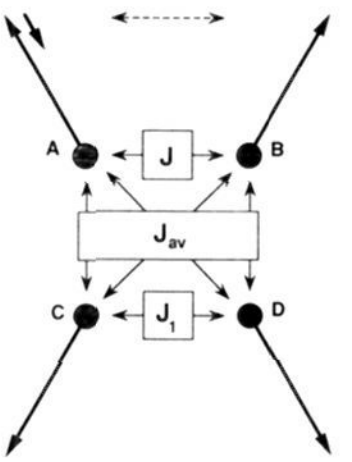

Figure 7. Exchange couplings figuring in the expression for the approximate exchange energy of the pair-delocalized configuration $|(S_{AB},S_{CD}{}^0)S\rangle^{\pm}$, given in eq 30.

depend on the exchange parameters for ferrous–ferric (J) and ferric–ferric interaction (J_1). The parameters in iron–sulfur clusters are negative and lead in dimeric clusters to an antiferromagnetic alignment of the iron spins. The exchange coupling constants in the ferric pairs of these systems are considerably larger in magnitude than those in the mixed-valence pairs. The most reliable estimates of their values are obtained from magnetic measurements on dimeric clusters, which exhibit localized mixed-valence states, resulting in values of $J \leq -160$ cm^{-1} and $J_1 \leq -360$ cm^{-1}.[16]

Homogeneous HDVV exchange ($J = J_1$), which is represented by the operator

$$H_{hom} = -(J/2)S^2 \tag{29a}$$

shifts the energies of all states with the same spin number S by an equal amount of energy, $-JS(S + 1)/2$, and stabilizes, for negative J values, the spin states in the order $E(1/2) < E(3/2) < \ldots < E(19/2)$. Inhomogeneous HDVV exchange, arising for $\Delta J = J - J_1 \neq 0$, represented by the operator

$$H_{inhom} = (\Delta J/2)S_{klm}{}^2 \tag{29b}$$

(see eq 5), splits, however, also the level energies inside the manifolds of equal total spin. As before, we shall consider the cases of weak ($|\beta|/(\lambda^2/2\kappa) \ll 1$) and of strong positive transfer interaction ($\beta/(\lambda^2/2\kappa) > 1$) separately.

The electronic eigenstates of $H_{HDVV} = H_{hom} + H_{inhom}$, in absence of intercenter resonance ($\beta = 0$), are given in eq 1 and describe an excess electron which is strictly localized at one of the sites A, B, C, or D of the tetramer. The exchange interaction removes the degeneracy of the spin-state energies and results in the energy level scheme, with four-fold orbitally degenerate levels, given in eq 5. The largest exchange stabilization energies, in the parameter range relevant to iron–sulfur clusters, i.e., $J < 0$ and $J - J_1 > 0$, are attained in the state $|(S_A = 2, S_{BCD}{}^0 = 3/2)S = 1/2\rangle$ for $2J < J_1$ and in $|(S_A = 2, S_{BCD}{}^0 = 1/2)S = 3/2\rangle$ for $2J > J_1$. The localized ground state calculated from the aforementioned exchange parameters has spin $S = 3/2$ and lies 60 cm^{-1} below the energy of the $S = 1/2$ state. We notice, however, that neither of the localized states is compatible with the spectroscopic data of the oxidized HiPIP (see Introduction).

We shall now consider the effect of the HDVV exchange on states and energies of systems with strong transfer interaction. It was shown in the previous section that the electronic eigenstates at the minima of the adiabatic surfaces are simple linear combinations of configurations of the form $|(S_{AB},S_{CD}{}^0)S\rangle^{\pm}$ and $|(S_{AB}{}^0,S_{CD})S\rangle^{\pm}$. Obviously, the exchange energy of an eigenstate receives its main contribution from the principal component. The exchange energies of the configurations can be cast in a simple form, eq 30, by approximating the interpair coupling parameters, J_{AC}, J_{AD}, J_{BC}, and J_{BD}, by the average $J_{av} = (J + J_1)/2$ (see Figure 7):

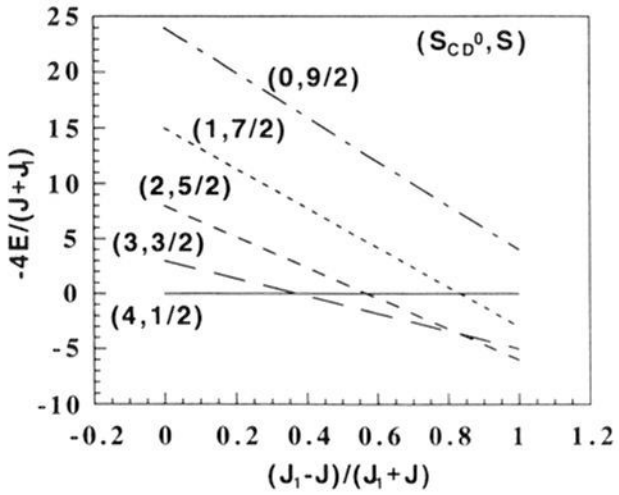

Figure 8. Relative exchange energies of the configurations $|(S_{AB} = 9/2,S_{CD}^0)S = 9/2 - S_{CD}^0\rangle^{\pm}$ as a function of the dispersion of J and J_1 in the range $J_1 < J < 0$, relevant to iron–sulfur clusters.

Table 3. Relative Exchange Energies, Vibronic Energies, and Total Energies of the Six Lowest-Energy, Broken-Symmetry, $S = 1/2$ States, Calculated in Different Approximations

eigenstates	ΔE_{HDVV}			ΔE_{vc}		ΔE_{tot}	
(9/2,4)[a]	0[b]	0[c]	0[d]	0[e]	0[f]	0 (1)[g]	0[h]
(7/2,3)	50	59	50	133	149	183 (2)	199
(5/2,2)	100	124	73	233	300	333 (3)	373
(5/2,3)	400	330	246	208	259	608 (6)	505
(7/2,4)	450	389	313	111	123	561 (5)	436
(9/2,5)	500	444	393	−14	−13	486 (4)	380

[a] Principal component, $|(S_{AB},S_{CD}^0)1/2\rangle^-$, of eigenstate in symmetry-adapted representation. [b] Energy of principal component obtained from eq 30 using $\Delta J = 200$ cm^{-1}. [c] Energy of principal component obtained from eq 29b using $\Delta J = 200$ cm^{-1}. [d] Obtained by full calculation. [e] Evaluated from last column of Table 2. [f] Obtained by full calculation for $\Delta J = 0$. [g] Column 2 + column 5. Energy order in parentheses. [h] Obtained by full calculation or by addition: column 4 + column 6.

$$E(S_{AB},S_{CD}^0,S) = E^0 + [(J_1 - J)/4]S_{AB}(S_{AB} + 1) + [(J - J_1)/4]S_{CD}^0(S_{CD}^0 + 1) - [(J + J_1)/4]S(S + 1) \quad (30)$$

As we shall show later on, the basic trends in the effect of HDVV exchange on state energies are already reproduced by eq 30. Let us examine the case $J_1 \leq J \leq 0$ relevant to iron–sulfur clusters. The coefficients of the three terms in eq 30 are then negative, positive, and positive, respectively. The sum of the first two terms is negative for $S_{AB} > S_{CD}^0$ and positive otherwise. Consequently, the configuration $|(S_{AB},S_{CD}^0)S\rangle$ has for $S_{AB} > S_{CD}^0$ lower energy than for $S_{AB} < S_{CD}^0$ (see also ref 15). The largest exchange stabilization energy for a given spin number S is reached for $S_{AB} = 9/2$ and $S_{CD}^0 = |S_{AB} - S|$. Hence, the ground configuration belongs to the series $|(9/2,4)1/2\rangle^-$, $|(9/2,3)3/2\rangle^-$, ... The configuration which is actually lowest depends on the values of J and J_1. Figure 8 shows that the low-spin configuration $|(9/2,4)1/2\rangle^-$ lies lowest in energy in the case of a moderate dispersion of the values for J and J_1 ($(J_1 - J)/(J_1 + J) < 3/8$). For larger dispersions, configurations of higher spin ($S = 3/2$ and $5/2$) are favored by inhomogeneous exchange. The aforementioned exchange parameters correspond to a location near the crossing of the $S = 1/2$ and $S = 3/2$ levels. The exchange-coupling constants in the tri- and tetrameric clusters may, of course, differ from those in the dimeric units. If we assume that their values fulfil the inequality $(J_1 - J)/(J_1 + J) < 3/8$, i.e., the coupling constants in tetramers are less dispersed than those in dimers, then the antiferromagnetic exchange will stabilize an electronic broken-symmetry state of low spin with principal component $|(9/2,4)1/2\rangle^-$.

It is also of interest to consider the effect of inhomogeneous exchange on the energies of the other $S = 1/2$ levels. Table 3 (column 2) presents the relative exchange energies of the principal configurations (column 1) of the six energetically lowest electronic states of spin $S = 1/2$ as obtained from eq 30, by adopting the

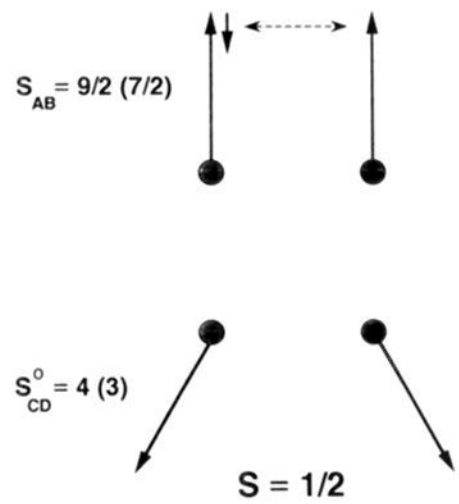

Figure 9. Schematic representation of the spin structure of the principal component of the broken-symmetry, $S = 1/2$ ground state obtained for $\beta/(\lambda^2/2\kappa) \gtrsim 1$. The spins S_{AB} and S_{CD}^0 figuring in the component are indicated. The values in parentheses refer to the first excited state.

value $J - J_1 = 200$ cm^{-1}. As stated before, the largest exchange stabilization energy is obtained in the configuration $|(9/2,4)1/2\rangle^-$. The principal component, $|(9/2,5)1/2\rangle^-$, of the ground state calculated without HDVV exchange lies 500 cm^{-1} above the lowest exchange level. In order to evaluate the relative values of the total energies, the relative exchange energies (column 2) and vibronic energies (column 5) must be added (column 7). Since the vibronic energy of the broken-symmetry state of $|(9/2,5)1/2\rangle^-$-type is only 14 cm^{-1} below that of $|(9/2,4)1/2\rangle^-$-type, the inhomogeneous HDVV exchange can stabilize the latter as the ground state. Furthermore, it will be seen from Table 3 that the first excited state is of $|(7/2,3)1/2\rangle^-$ character. Thus, the set of spin structures deduced from the total Hamiltonian in the two energetically lowest broken-symmetry eigenstates (see Figure 9) encloses the ground-state structures inferred from spectroscopic studies on oxidized HiPIP and its synthetic analogues (see Introduction).

So far, the effect of the HDVV interaction on state energies was simply accounted for by adding the approximate exchange energies, given by eq 30, to the energy eigenvalues of the Hamiltonian $H_t + H_{ev} + H_{el}$. This procedure rests on the following premises: (i) the eigenstates of $H_t + H_{ev} + H_{el}$ are not altered by inhomogeneous HDVV exchange, (ii) the exchange energies of the minority components of the eigenstates are negligible, (iii) nondiagonal HDVV interactions between different eigenstates have a vanishing effect on state energy, and (iv) the exchange couplings between the mixed-valence pair and the pure-valence pair can be described by a single parameter, J_{av}. In order to verify the validity of these premises, we calculated the eigenvalues and eigenstates of the operator $H_t + H_{ev} + H_{el} + H_{inhom}$, i.e., of the former three interactions in the presence of the genuine inhomogeneous HDVV operator, eq 29b, by means of the procedure outlined in the Description of the Model section (i.e., full calculation). The eigenvectors thus obtained are linear combinations of the localized basis states given in eq 1. It is more convenient, however, to analyze the exchange effect on state composition in symmetry-adapted representation. The delocalized basis states can be expressed in the localized basis by single vector-recoupling operations in the right-hand size of eq 14, leading, in eq 14a, to the relation

$$|(S_{AB},S_{CD}^0)S\rangle^{\pm} = \sum_{S_3^0} \langle (S_A,(S_B^0,S_{CD}^0)S_3^0)S|((S_A,S_B^0)S_{AB},S_{CD}^0)S\rangle \times (1/\sqrt{2})[|(S_A,(S_B^0,S_{CD}^0)S_3^0)S\rangle \pm (-1)^{S_{AB}+1/2}|(S_B,(S_A^0,S_{CD}^0)S_3^0)S\rangle] \quad (31)$$

A similar expression can be derived for the functions given in eq 14b. The summation in eq 31 is over S_3^0 ($= S_{ACB}^0 = S_{BCD}^0$) and is constrained by the triangular condition $|S_A - S_3^0| \leq S \leq |S_A$

Table 4. Expansion of Symmetry-Adapted Basis States of Spin $S = 1/2$ in Localized Basis

symmetry-adapted basis state	expansion in localized basis
$\|(1/2,0)1/2\rangle^{\pm}$ [a]	$\|0,5/2,1/2\rangle^{\mp}$ [b]
$\|(1/2,1)1/2\rangle^{\pm}$	$-(8/15)^{1/2}\|1,3/2,1/2\rangle_{\mp} + (7/15)^{1/2}\|1,5/2,1/2\rangle_{\mp}$
$\|(3/2,1)1/2\rangle^{\pm}$	$(7/15)^{1/2}\|1,3/2,1/2\rangle_{\pm} + (8/15)^{1/2}\|1,5/2,1/2\rangle_{\pm}$
$\|(3/2,2)1/2\rangle^{\pm}$	$-(3/5)\|2,3/2,1/2\rangle_{\pm} + (4/5)\|2,5/2,1/2\rangle_{\pm}$
$\|(5/2,2)1/2\rangle^{\pm}$	$(4/5)\|2,3/2,1/2\rangle_{\mp} + (3/5)\|2,5/2,1/2\rangle_{\mp}$
$\|(5/2,3)1/2\rangle^{\pm}$	$-(8/35)^{1/2}\|3,3/2,1/2\rangle_{\mp} + (27/35)^{1/2}\|3,5/2,1/2\rangle_{\mp}$
$\|(7/2,3)1/2\rangle^{\pm}$	$(27/35)^{1/2}\|3,3/2,1/2\rangle_{\pm} + (8/35)^{1/2}\|3,5/2,1/2\rangle_{\pm}$
$\|(7/2,4)1/2\rangle^{\pm}$	$-(1/3)\|4,3/2,1/2\rangle_{\pm} + (8/9)^{1/2}\|4,5/2,1/2\rangle_{\pm}$
$\|(9/2,4)1/2\rangle^{\pm}$	$(8/9)^{1/2}\|4,3/2,1/2\rangle_{\mp} + (1/3)\|4,5/2,1/2\rangle_{\mp}$
$\|(9/2,5)1/2\rangle^{\pm}$	$\|5,5/2,1/2\rangle_{\mp}$

[a] $|(S_{AB},S_{CD}^0)S\rangle^{\pm}$. [b] $|S_{CD}^0,S_3^0,S\rangle_{\pm}$, see text.

Table 5. Compositions of the Six Lowest-Energy Eigenstates of Spin $S = 1/2$ in Symmetry-Adapted Representation Obtained with and without HDVV Exchange

composition of eigenstates[a]				sum
		$\Delta J = 200$ cm^{-1}		
92(9/2,4)$^-$ [b]	8(4,7/2)$^+$	0(4,9/2)$^-$	0(7/2,4)$^+$	100
82(7/2,3)$^-$	16(3,5/2)$^+$	1(3,7/2)$^-$	1(5/2,3)$^+$	100
69(5/2,2)$^-$	25(2,3/2)$^+$	2(2,5/2)$^-$	4(3/2,2)$^+$	100
92(9/2,5)$^-$	8(4,9/2)$^+$			100
84(7/2,4)$^-$	15(3,7/2)$^+$			99
75(5/2,3)$^-$	22(2,5/2)$^+$			97
		$\Delta J = 0$		
92(9/2,4)$^-$	8(4,7/2)$^+$	0(4,9/2)$^-$	0(7/2,4)$^+$	100
84(7/2,3)$^-$	16(3,5/2)$^+$	0(3,7/2)$^-$	0(5/2,3)$^+$	100
75(5/2,2)$^-$	25(2,3/2)$^+$	0(2,5/2)$^-$	0(3/2,2)$^+$	100
93(9/2,5)$^-$	7(4,9/2)$^+$			100
85(7/2,4)$^-$	15(3,7/2)$^+$			100
78(5/2,3)$^-$	22(2,5/2)$^+$			100

[a] Calculated for $\lambda^2/2\kappa = 2000$ cm^{-1}, $\beta = 10^4$ cm^{-1}, $J = 0$, and ΔJ indicated at the minimum $Q_x^0/(\lambda/\kappa) = 0.4276$, $Q_y^0 = Q_z^0 = 0$ of the lowest state, which is of $(9/2,5)^-$-type, obtained for $\Delta J = 0$. [b] Weight (%) of symmetry-adapted basis state $|(S_{AB},S_{CD}^0)1/2\rangle^{\pm}$.

$+ S_3^0|$; thus for $S_A = 2$ and $S = 1/2$, one obtains $S_3^0 = 1/2$ and $3/2$. The resulting expressions for the delocalized basis states of spin $S = 1/2$, with the excess electron occupying AB, are explicitly given in Table 4. The +/− combinations of the two localized functions occurring in the right-hand side of eq 31 are indicated in Table 4 by the notation $|S_{CD}^0,S_3^0,S\rangle_{\pm}$. The exchange energies of these latter functions are given by eq 5. The inhomogeneous exchange energies (eq 29b) of the symmetry-adapted basis states are calculated by weighted addition of the energies $(15/8)\Delta J$ and $(35/8)\Delta J$ of the $S_3^0 = 3/2$ and $S_3^0 = 5/2$ terms, respectively. We note that these energies are independent of the label ±. The relative values of the exchange energies thus obtained for the principal components indicated in Table 3 are given in column 3. Comparison of the latter values with those given in column 2 of the same table indicates that the averaging procedure resulting in J_{av} has a moderate but nonnegligible effect on the calculated exchange splittings (see point iv, above). The compositions, in symmetry-adapted representation, of the electronic eigenstates of spin $S = 1/2$ calculated by the full treatment, using a representative set of model parameters, are indicated in Table 5 (columns 1–4). The upper part of the table refers to the values $J = 0$ and $J_1 = -200$ cm^{-1} ($\Delta J = 200$ cm^{-1}) and the lower part to $J = J_1 = 0$. Comparison reveals that the eigenstates are hardly affected by exchange interaction (see point i, above). As a consequence, the positions of the adiabatic potential minima in Q space remain virtually unchanged too. Subtraction of the total energies (not given) calculated for the corresponding states in the upper and lower part of the table (i.e., those having the same principal component indicated in column 1) yields the exchange energy of the state concerned. The relative values of the exchange energies thus obtained are given in Table 3 (column 4) and show overall somewhat smaller values than the exchange splittings between the principal components (column 3), indicating that the premises ii or iii given above are not quite fulfilled. The relative vibronic energies of the broken-symmetry states given in Table 5 for $\Delta J = 0$, resulting from full calculation, are presented in Table 3 (column 6). Comparison of the latter set of numbers and the vibronic energies obtained in the limit $\beta/(\lambda^2/2\kappa) \rightarrow \infty$ (column 5) reveals the persistence of some pseudo-Jahn–Teller interaction for the parameter values adopted in Table 5. The last column of Table 3 contains the relative values of the total energies of the broken-symmetry states given for $\Delta J = 200$ cm^{-1} in Table 5 as obtained by full calculation. These values can also be evaluated by adding the exchange and vibronic energies given in columns 4 and 6. The approximated splitting energies between the three lowest levels of spin $S = 1/2$ (column 7) are in good agreement with the results of the full calculation (last column). The deviations in the energies of the upper three states are larger but do not alter the energy order.

Conclusion

We analyzed the magnetic and electronic properties of the oxidized HiPIP in the framework of the phenomenological approach, which was successfully applied previously to the interpretation of the properties of reduced ferredoxin II. The main results of the present work can be summarized as follows.

(i) The electronic ground state of the transfer operator of the regular tetrahedral mixed-valence system $Fe(II)Fe(III)_3$ is, for $\beta < 0$, an orbitally nondegenerate state of maximum spin. The electronic ground state obtained for $\beta > 0$ is highly degenerate, including states of different spin and orbital degeneracy.

(ii) The vibronic interactions of the excess electron with local, symmetric ligand shell distortions give rise to various localization patterns depending on the value of the ratio $\beta/(\lambda^2/2\kappa)$. For small ratios, $|\beta/(\lambda^2/2\kappa)| \ll 1$, the excess electron is trapped at one site of the cluster. For $\beta/(\lambda^2/2\kappa) > 1$, the probability densities of the excess electron in states of lower spin number are mainly concentrated at two equivalent sites of the cluster (pair delocalization). For large, negative values of the ratio, the excess electron charge is uniformly distributed over the cluster.

The conclusions formulated under (i) and (ii) above parallel those deduced for the trimeric mixed-valence unit d^5-d^5-d^6 in ferredoxin II.

(iii) The excess-electron charges in the pair-delocalized states obtained for $\beta/(\lambda^2/2\kappa) > 1$ are not strictly confined to the majority pair. Their occupation numbers depend on spin and lead to vibronic energies which appear in the order (S=) $1/2 < 3/2 <$ .... Moreover, vibronic interaction removes the degeneracies of the electronic state energies within the ground manifolds of given spin. The two lowest states of spin $S = 1/2$, thus obtained, have principal components $|(9/2,5)1/2\rangle^-$ (ground) and $|(9/2,4)1/2\rangle^-$.

(iv) Inhomogeneous HDVV exchange has little effect on state composition and on adiabatic minimum position in Q space. On the contrary, its effect on state energy is considerable. The two lowest broken-symmetry states evaluated by adopting a set of exchange-coupling constants representative for iron–sulfur clusters have $|(9/2,4)1/2\rangle^-$ (ground) and $|(7/2,3)1/2\rangle^-$ character. Ground states of similar character have been inferred from the spectroscopic studies of the HiPIP and synthetic analogues thereof.

The parameter range, $\beta/(\lambda^2/2\kappa) \geq 1$, following from the interpretation of the pair-delocalized, $S = 2$ ground state in reduced ferredoxin II,[50] coincides with that deduced here for HiPIP. As expected, the basic interactions have, apparently, not drastically changed, i.e., not to the extent that the sign of β is reversed, in passing from trimeric to tetrameric clusters.

The analyses of ferredoxin II in ref 50 and of HiPIP presented here differ in one point. In the former, a ground state of correct spin structure is already obtained from double-exchange and vibronic coupling alone, whereas the latter has to invoke

inhomogeneous HDVV exchange in order to distinguish the state of $|(9/2,4)1/2\rangle^-$ character from that of $|(9/2,5)1/2\rangle^-$ character.

The results presented in this article provide new evidence for the correctness of our basic assumptions about the spin-state and electron distribution regulating mechanisms which underlie the electronic structures in iron–sulfur clusters.

Appendix

The transfer matrices are readily evaluated in symmetry-adapted representation (eq 14a,b) by utilizing the following two selection rules.

The *first* rule reads

$$\Delta S_{AB}{}^0 = \Delta S_{CD}{}^0 = 0 \qquad \text{(A.1a)}$$

and follows from the commutation relations $[H_t,S_{AB}{}^0] = [H_t,S_{CD}{}^0] = 0$.

The *second* rule states that interdimer interactions $\langle\phi_-{}^{AB}|H_t|\phi_\pm{}^{CD}\rangle$ and $\langle\phi_-{}^{CD}|H_t|\phi_\pm{}^{AB}\rangle$ are zero. This rule is a consequence of the eqs A.1b,c and the orthogonality relation $\langle\phi_+{}^{AB}|\phi_-{}^{CD}\rangle = \langle\phi_-{}^{AB}|\phi_+{}^{CD}\rangle = 0$:

$$H_t\phi_-{}^{AB} = -\beta\phi_-{}^{AB} \qquad \text{(A.1b)}$$

$$H_t\phi_-{}^{CD} = -\beta\phi_-{}^{CD} \qquad \text{(A.1c)}$$

Another useful set of relations in the calculation of the matrix elements is given by

$$H_t\phi_+{}^{AB} = \beta\phi_+{}^{AB} + 2\beta\phi_+{}^{CD} \qquad \text{(A.2a)}$$

$$H_t\phi_+{}^{CD} = \beta\phi_+{}^{CD} + 2\beta\phi_+{}^{AB} \qquad \text{(A.2b)}$$

The construction of the Hamiltonian matrices, using the selection rules, will be illustrated from an example. Let us calculate the interaction matrix involving the basis state

$$|(S_{AB} = 9/2,S_{CD}{}^0 = 4)S = 1/2\rangle^- = (11/12)^{1/2}|((S_{AB}{}^0 = 5,s = 1/2)S_{AB} = 9/2,S_{CD}{}^0 = 4)S = 1/2;\phi_-{}^{AB}\rangle + (1/12)^{1/2}|((S_{AB}{}^0 = 4,s = 1/2)S_{AB} = 9/2,S_{CD}{}^0 = 4)S = 1/2;\phi_+{}^{AB}\rangle \qquad \text{(A.3)}$$

The action of the transfer operator on the first configuration, containing $\phi_-{}^{AB}$, yields no interdimer transfer (second rule). Its action on the second term gives rise to interdimer transfer involving the configurations (first rule)

$$|((S_{AB}{}^0 = 4,(s = 1/2,S_{CD}{}^0 = 4)S_{CD} = 9/2)S = 1/2;\phi_+{}^{CD}\rangle \qquad \text{(A.4a)}$$

$$|((S_{AB}{}^0 = 4,(s = 1/2,S_{CD}{}^0 = 4)S_{CD} = 7/2)S = 1/2;\phi_+{}^{CD}\rangle \qquad \text{(A.4b)}$$

in which the excess electron occupies the orbital $\phi_+{}^{CD}$. They interact, in their turn, with the configuration

$$|((S_{AB}{}^0 = 4,s = 1/2)S_{AB} = 7/2,S_{CD}{}^0 = 4)S = 1/2;\phi_+{}^{AB}\rangle \qquad \text{(A.4c)}$$

with the electron being once again at the pair AB. In summary, there result transfer interactions between the symmetry-adapted basis states

$$|(9/2,4)1/2\rangle^- = |(S_{AB} = 9/2,S_{CD}{}^0 = 4)S = 1/2\rangle^- \qquad \text{(A.5a)}$$

$$|(4,9/2)1/2\rangle^- = |(S_{AB}{}^0 = 4,S_{CD} = 9/2)S = 1/2\rangle^- \qquad \text{(A.5b)}$$

$$|(7/2,4)1/2\rangle^+ = |(S_{AB} = 7/2,S_{CD}{}^0 = 4)S = 1/2\rangle^+ \qquad \text{(A.5c)}$$

$$|(4,7/2)1/2\rangle^+ = |(S_{AB}{}^0 = 4,S_{CD} = 7/2)S = 1/2\rangle^+ \qquad \text{(A.5d)}$$

in which the latter three states contain the configurations of eqs A.4a, A.4c, and A.4b, respectively.

The evaluation of the matrix elements involves spin projection factors of the form

$$\langle((S_{AB}{}^0,s)S_{AB},S_{CD}{}^0)S|((S_{AB}{}^0,(s,S_{CD}{}^0)S_{CD})S\rangle = (2S_{AB} + 1)^{1/2}(2S_{CD} + 1)^{1/2}W(S_{AB}{}^0,s,S,S_{CD}{}^0;S_{AB},S_{CD}) \qquad \text{(A.6)}$$

where W is a Racah coefficient, which can be readily calculated from the standard expression.[54] Furthermore, by taking into account the factor 2β in eq 16, the coefficients weighting the configurations in eqs 14a,b, and the overall multiplication factor of 6/5 imposed by the coupled core-spin representation, we arrive at the interaction matrix given by eq 15 of the text.

(54) Brink, D. M.; Satchler, G. R. *Angular Momentum*; Oxford Library of Physical Sciences; Clarendon: Oxford, U.K., 1968.